International Journal of Nanomedicine

Dovepress

open access to scientific and medical research

Open Access Full Text Article

ORIGINAL RESEARCH

Ultrasound Triggered Tumor Metabolism Suppressor Induces Tumor Starvation for Enhanced Sonodynamic Immunotherapy of Breast Cancer

Kun Qiao[1,*], Cheng Luo[2,*], Rong Huang[3,4], Jingfeng Xiang[5], You Pan[3,4], Shiyuan Zhang[1], Cong Jiang[1], Shuaijie Ding[6], Huawei Yang[3,4], Yuanxi Huang[1], Shipeng Ning[3,4]

[1]Department of Breast Surgery, Harbin Medical University Cancer Hospital, Harbin, 150081, People's Republic of China; [2]Department of Anesthesiology, The Maternal and Child Health Hospital of Guangxi Zhuang Autonomous Region, Nanning, 530000, People's Republic of China; [3]Guangxi Medical University Cancer Hospital, Nanning, 530000, People's Republic of China; [4]Key Laboratory of Breast Cancer Diagnosis and Treatment Research of Guangxi Department of Education, Nanning, 530000, People's Republic of China; [5]Department of General Surgery & Guangdong Provincial Key Laboratory of Precision Medicine for Gastrointestinal Tumor, Nanfang Hospital, The First School of Clinical Medicine, Southern Medical University, Guangzhou, Guangdong, 510515, People's Republic of China; [6]Department of Gastrointestinal Surgery & Department of Geriatrics, Shenzhen People's Hospital (The Second Clinical Medical College, Jinan University, The First Affiliated Hospital, Southern University of Science and Technology), Shenzhen, Guangdong, 518020, People's Republic of China

*These authors contributed equally to this work

Correspondence: Shipeng Ning; Yuanxi Huang, Email nspdoctor@163.com; rxwk@163.com

Introduction: Sonodynamic therapy (SDT) as an emerging tumor treatment gained wide attention. However, tumor vascular destruction and oxygen depletion in SDT process may lead to further hypoxia. This may lead to enhanced glycolysis, lactate accumulation, and immunosuppression.

Methods: A glycolysis inhibitor (3PO) loaded and PEG modified black phosphorus nanosheets (BO) is constructed for potent starvation therapy and efficient immune activation.

Results: Under ultrasound irradiation, the BO can produce ROS to destroy tumors and tumor blood vessels and lead to further hypoxia and nutrients block. Then, the released 3PO inhibits tumor glycolysis and prevents the hypoxia-induced glycolysis and lactate accumulation. Both SDT and 3PO can cut off the source of lactic acid, as well as achieve antitumor starvation therapy through the blockade of the adenosine triphosphate (ATP) supply. In addition, the combination of starvation treatment and SDT further facilitates dendritic cells (DC) maturation, promotes antigen presentation by DCs, and eventually propagates the antitumor immunity and inhibition of abscopal tumor growth.

Conclusion: This is the first time that combines SDT with inhibition of glycolysis, achieving admirable tumor treatment and decreasing adverse events caused by SDT process and that has caused good immune activation. Our system provides a new idea for the future design of anti-tumor nanomedicines.

Keywords: sonodynamic therapy, glycolysis inhibitor, black phosphorus nanosheets, starvation therapy, immune activation

Introduction

Owing to low clinic treatment efficacy, adverse effects and poor precision, cancer therapy is always a tremendous challenge.[1–3] Sonodynamic therapy (SDT) is an emerging and precision-guided modality with high tissue-penetration depth, non-invasive influence and low cost that is expected to realize ablation of solid tumors.[4–7] During the treatment of appropriate SDT, sonosensitizers promote activity of nearby molecular oxygen (O_2) in the tumor microenvironment (TME) and convert O_2 to singlet oxygen ($^1O_2$) (one of the reactive oxygen species (ROS)) which could destroy tumor cells.[8,9] Although SDT possesses analogous principle with photodynamic therapy (PDT),[10–12] ultrasound is more safe compared with light, but more importantly, it can penetrate deeper into tissue, up to 10 cm.[13] In our recent study, a glutathione (GSH)-suppressing nanoplatelets were developed to boost the efficacy of SDT.[14] We first load oxidative stress amplifier cinnamaldehyde and

Received: 5 April 2023
Accepted: 26 June 2023
Published: 10 July 2023

sonosensitizers IR780 to the pores of mesoporous silica nanoparticles, then the surface of hybrid nanoparticles were coated with platelet membranes. Membranes of platelets could endow nanoparticles with long blood circulation, immune escape capability and tumor targeting ability. The in vitro and in vivo experiments confirm that this novel enhanced SDT is innoxious and high-performance. Likewise, Sun et al designed a liposome loaded with DVDMs and modified with IRGD (iRGD-Lipo-DVDMS) in combination with ultrasound-targeted microbubble destruction (UTMD) to irradiate glioma nerves with low intensity focused ultrasound (FUS) to enhance the efficacy of SDT.[15] However, as a principal characteristic of solid tumors, hypoxia severely limits the therapy efficiency of SDT,[6,16–18] it has been reported that blood vessel destruction during SDT will further aggravate tumor hypoxia.[10,13] This will undoubtedly exert a serious impact on the therapeutic effect of SDT.

Hypoxia condition in tumor tissues would also exacerbate lactic acid accumulation.[19,20] Furthermore, lactic acid, which originally exists in large quantities in TME, will cause the voracious growth of tumor cells. Tumor cells are constantly absorbing glucose and converting it into lactic acid with glycolysis (Warburg effect).[21,22] Tumors use this rapid metabolism to promote their proliferation and metastasis, and their lactic acid release has an important role in the regulation of tumor immune microenvironment.[20] This abnormal tumor lactate metabolism would promote the invasion and metastasis of tumors and the formation of new blood vessels, and maintain the tumor immunosuppressive microenvironment by regulating the transformation of macrophages to M2 type and reducing the killing function of (natural killer) NK cells.[23,24] Dendritic cells (DCs) are modulators of the anti-tumor immune response of T cells by loading tumor-associated antigens (TAAs) as peptides on major histocompatibility complex (MHC) molecules.[25–29] However, the accumulation of lactic acid produced by tumor cells could further damage cytotoxic T cells and inhibit the differentiation and maturation of DCs, which would exert adverse influences to immune response.[19,30,31] As the most clinically promising treatment at present, cancer immunotherapy, the activity of DC cells undoubtedly affect the treatment. Both the physical and biochemical properties of the nanodrugs can be exploited to obtain optimal and expected tumor killing and cell uptake. Some progress has been made in nanomedicines-mediated cancer immunotherapy.[32–35] However, in spite of recent advances, few studies have been conducted to modulate the content of DC cells by decreasing lactic acid content in TME.

Due to its good biocompatibility and photothermal effect, black phosphorus nanosheets (BP NSs) have been widely used in biological applications and tumor photothermal therapy,[36–38] only a few studies have applied BP in sonodynamic therapy.[39,40] Herein, we loaded a glycolysis inhibitor (3PO), a promising inhibitor of glycolytic pathway, onto black phosphorus nanosheets to develop an integrated, noninvasive and biocompatible platform that would allow both effective SDT and immune activation (Figure 1). BP nanosheets act as a smart gatekeeper to simultaneously facilitate the loading and delivery of the 3PO. In addition, as a novel sonosensitizer, BP can generate ROS under appropriate ultrasound stimulation to kill tumor cells and destroy tumor blood vessels, leading to further hypoxia and nutrients block. Simultaneously, 3PO could suppress the procedure of tumor glycolysis and achieve profound starvation therapy through blockading supply of the adenosine triphosphate (ATP). Furthermore, this starvation treatment-mediated dual lactic acid depletion effect and tumor-associated antigen (TAA) release facilitates dendritic cell (DC) maturation, promotes antigen presentation by DCs, and eventually propagates the antitumor immunity and inhibition of abscopal tumor growth.

To our best knowledge, this study firstly reports a combination of potent SDT and glycolysis inhibiting effect, as well as realizing good in vitro and in vivo antitumor therapy with excellent biocompatibility. Our BO system could act as a promising approach for the systemic immune activation without the employment of any immune agonists to treat cancer and provides a new idea for the future design of anti-tumor nanomedicines.

Materials and Methods

Cell Line

4T1 mouse breast cancer cell line was obtained from the Cell Bank of the Chinese Academy of Sciences and incubated in RPMI-1640 medium supplemented with 10% FBS in a humidified atmosphere at 37°C in an incubator under normoxic circumstances (pO_2: 21%; 5% CO_2) or in a hypoxic incubator (pO_2: 2%; 2% O_2, 93% N_2, and 5% CO_2) (Moriguchi, Japan).

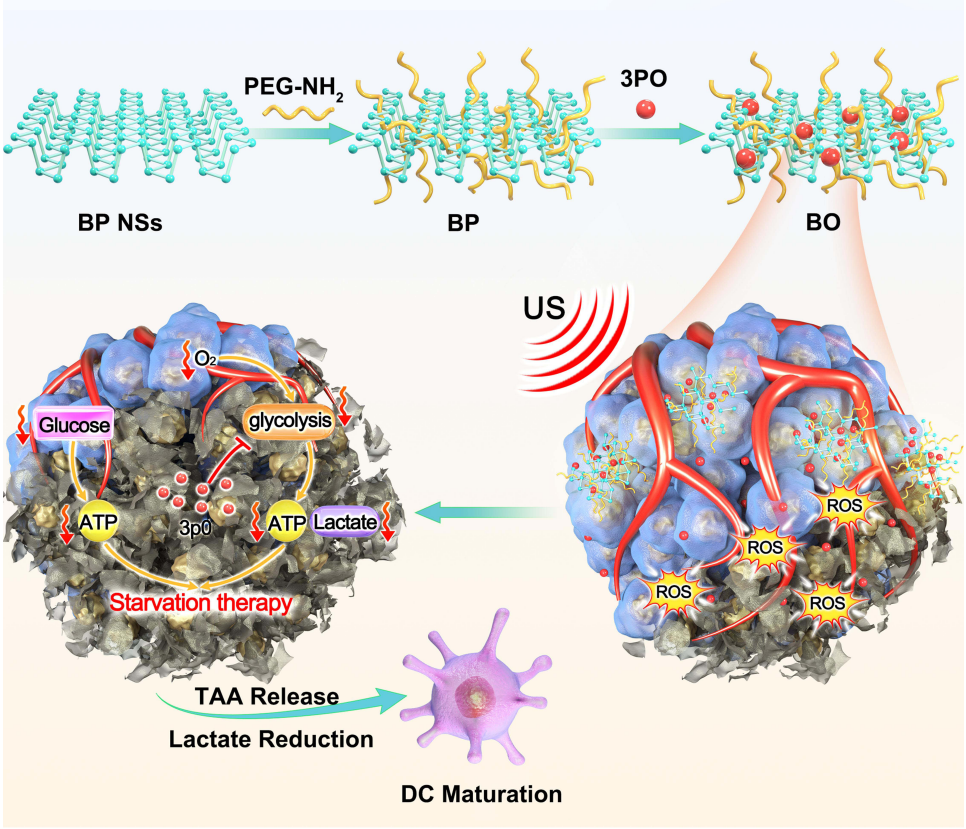

Figure 1 Schematic illustration of ultrasound triggered tumor metabolism suppressor induces tumor starvation for enhanced sonodynamic immunotherapy of breast cancer.

Animal Tumor Models

Female BALB/c aged 5–6 week were purchased from Vital River Company (Beijing, China). Balb/c mice were subcutaneous injected with 5×10^6 4T1 cells into the right flank (primary tumors) and 1×10^6 4T1 cells into the left flank (abscopal tumors), respectively. The animal experiments were carried out according to the protocol approved by the Ministry of Health in People's Republic of PR China and were approved by the Administrative Committee on Animal Research of the Shenzhen People's Hospital.

Preparation of PEG Modified BP NSs (BP)

BP NSs (1 mg) dispersed in 5 mL of H_2O were mixed with 5 mg of PEG-NH_2. After being sonicated for 30 min and stirred for 4 h, excess PEG molecules were removed by centrifugation.

Preparation and Characterization of 3PO Loaded BP (BO)

BP@PEG NS solution (3 mL, 50 ppm) in PBS at pH 7.4 was mixed with a dimethyl sulfoxide (DMSO) solution containing 100 μg/mL of 3PO (2 mL) and stirred for 24 h. The resulting suspension was centrifuged at 12000 rpm for 20 min and rinsed with PBS three times. 3PO loading capacity was calculated by UV-vis spectra at the UV-vis spectrophotometry Lambda 35 (Perkin-Elmer). Loading capacity = M_{3P0}/M_{BP}. where M refers to the mass, M = cV. c is the concentration and V is the volume of BO dispersion. The 3PO and BP concentration in BO dispersion was determined by UV− vis−NIR and the corresponding normalized absorbance. The zeta potential of BP NSs, BO and BP was measured by dynamic light scattering (DLS, Nano-Zen 3600, Malvern Instruments, UK).

Statistical Analysis

Experimental data were analyzed by using one-way ANOVA followed by the post-Tukey comparison tests with GraphPad Prism 5.0 software. P <0.05 indicates statistical difference. *$P < 0.01$, **$P < 0.005$, ***$P < 0.001$.

Results

Preparation and Characterization of BO System

Black phosphorus is a biodegradable two-dimensional multifunctional nanomaterial, which is widely used in photodynamic therapy, photothermal therapy and drug delivery.[41,42] As a metal-free layered semiconductor, BP nanosheet exhibits the thickness-dependent band gap tunable from about 0.3 eV for bulk to 2.0 eV for single layer.[40] Compared with other 2D materials such as graphene and MoS_2, MXenes, BP has much higher surface to volume ratio due to its puckered lattice configuration, which can increase the drug loading capacity.[43,44] As an emerging therapy, sonodynamic therapy (SDT) has the advantage of strong penetration depth,[45,46] so we thought of using black phosphorus as sonosensitizer and drug carrier to carry out our project. Li et al demonstrate BP nanosheet exhibited ultrasound-excited cytotoxicity to cancer cells via ROS generation, thereby suppressing tumor growth and metastasis without causing off-target toxicity in tumor-bearing mouse models.[40] The ultrasonic wave introduces mechanical strain to the BP nanosheet, leading to piezoelectric polarization which shifts the conduction band of BP more negative than $O_2/\cdot O_2^-$ while its valence band is more positive than $H_2O/\cdot OH$, thereby accelerating the ROS production. Figure S1 is transmission electron microscope (TEM) image of BP@PEG (BP) and BP NSs. We also tested TEM images after loading 3PO, as shown in Figure 2A. In order to prove the successful modification of PEG on BP NSs surface, we tested the zeta potential of BP, BP NSs and BO. As shown in Figure 2B, the Zeta potential value was significantly increased after modification of PEG, indicating the successful modification of PEG. The lateral size distribution of BO is shown in Figure S2 and BO is stable within three days (Figure S3). 3PO has an absorption peak at 309 nm, and we can also see the absorption peak of 3PO on the absorption spectrum of BO, indicating that 3PO has been successfully loaded onto BP (Figure 2C). The absorption peak of BP NSs at 700 cm^{-1} corresponds to the strong coupling vibration mode between phosphorus atoms in the black phosphorus lattice, and 1640 and 3450 cm^{-1} correspond to the variable-angle vibration and O-H stretching vibration of water molecules. The absorption peak of 3450 cm^{-1} in BP corresponds to the O-H stretching vibration of water molecule and the O-H or N-H bond stretching vibration of PEG molecule. The peak in the range of 3000–2800 cm^{-1} corresponds to the antisymmetric and symmetric telescopic vibrations of the methyl and methylene groups in PEG molecule. The absorption peak in the 1800–1700 cm^{-1} region corresponded to the C=O bond and C=C bond in PEG molecule. The absorption peak at 1450–1250 cm^{-1} corresponds to the bending vibration of CH_3 and CH_2 bonds. After modification by PEG, the bending vibration mode of P–P bond is strengthened. This is because the local charge distribution on the black phosphorus surface was changed due to PEG modification, making the P–P bond vibration more easily detected (Figure S4). The loading capacity of BO is about 15.3% in our experiments. ESR spectra showed that BP could produce singlet oxygen ($^1O_2$) and hydroxyl radicals (·OH) under ultrasonic irradiation (Figure 2D and E), which proved that BP could be used in sonodynamic therapy. Methylene blue degradation experiments also confirmed that BP and BO could produce highly toxic hydroxyl radicals under ultrasonic irradiation (Figures S5 and S6). Under ultrasonic irradiation, 3PO has a faster release rate, which may be caused by the heat and ROS produced by SDT (Figure 2F). After being cultured with 4T1 cells, a large number of BO entered the cells, indicating that BO had a good ability of cell internalization (Figure 2G). In general, we have successfully prepared BO system, which can be used in future biological experiments.

In vitro Anti-Tumor Study of BO System

After the successful preparation of BO, we eagerly carried out in vitro anti-tumor experiments. First of all, we verified the difference in the production of lactic acid by tumor cells under different oxygen conditions, as shown in Figure S7. After 24 h and 48 h of hypoxia treatment, the accumulation of lactic acid in tumor cells increased compared with that under aerobic conditions. This indicates that anaerobic conditions can promote glycolysis of cells and produce more lactic acid. In tumor tissue, lactic acid accumulation often causes some adverse reactions, such as tumor immunosuppression, recurrence, etc.[19,21] Therefore, hypoxia and lactic acid accumulation caused by photodynamic or SDT can be expected to cause these adverse reactions. We verified the generation of reactive oxygen species in tumor cells. As shown

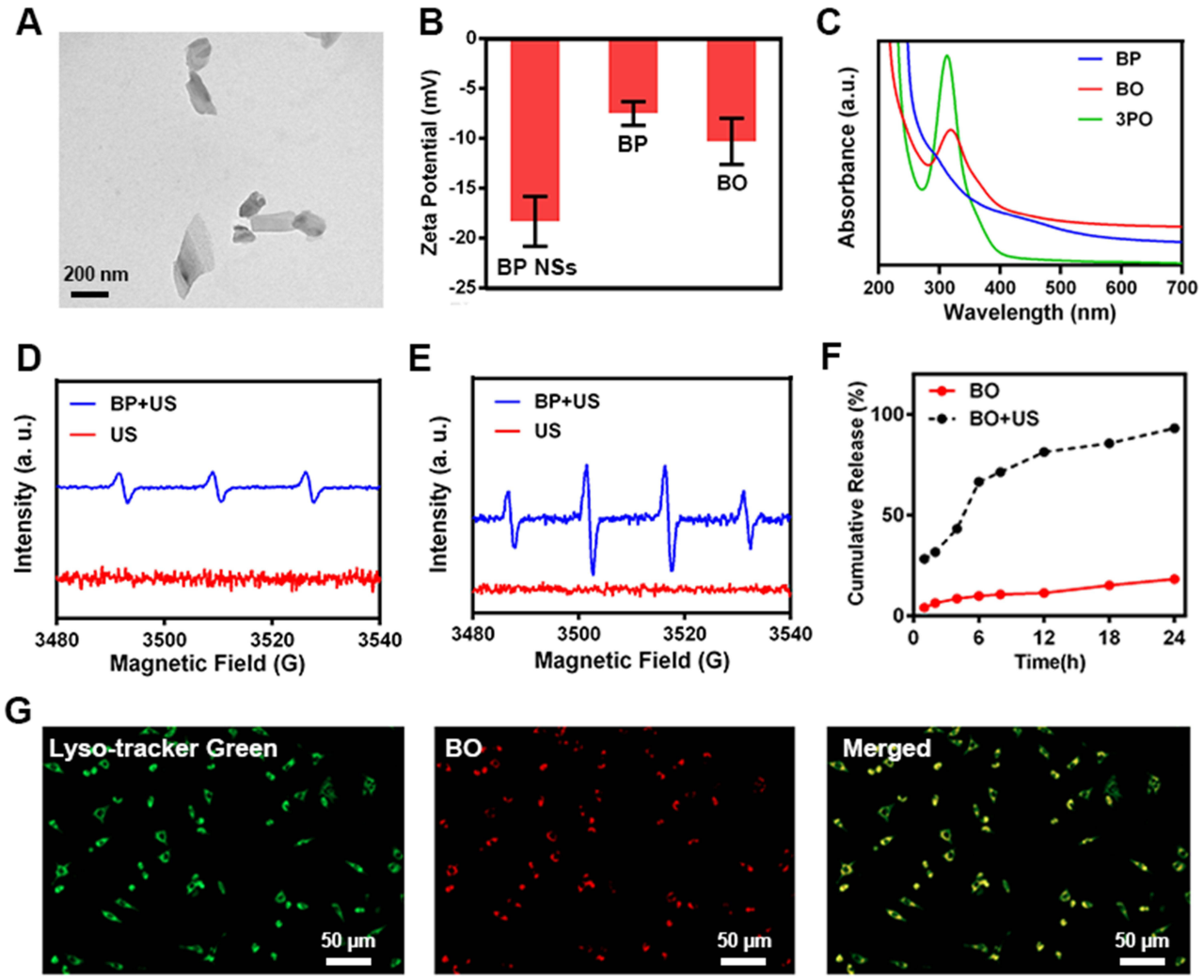

Figure 2 (**A**) TEM image of BO. (**B**) Zeta potential of BP NSs, BP and BO. (**C**) Absorbance spectrum of BP, 3PO and BO. (**D**) 1O2 and (**E**) •OH generation by PBS and BP with ultrasound (US) radiation using ESR. (**F**) 3PO release from BO with/without US radiation. (**G**) Fluorescence images of 4T1 cells (stained with Lyso-tracker Green) cultured with Cy5 labeled BO.

in Figure 3A, a large amount of ROS can be produced only in the presence of ultrasound and BP or BO, while BO alone or ultrasound can hardly produce ROS. Then we verified the SDT-induced tumor immunogenic cell death (ICD), as shown in Figure 3B and S4, under US, the BP and BO can induce immunogenicity cell death (ICD) characterized by high expression of calreticulin (CRT) on the surface of dying cancer cells, the cell fragments can also be a tumor associated antigen, which can effectively activate DC. Then, we verified the inhibitory effect of BO combined with acoustic dynamics on the production of lactic acid and ATP in tumor cells under hypoxia conditions. As shown in Figure 3C and D, after BO combined ultrasound, extracellular lactic acid content and intracellular ATP content decreased significantly. Compared with each control group, there are significant differences, indicating that sonodynamic therapy and 3PO mediated glycolysis inhibition can effectively inhibit the respiration of tumor cells and inhibit tumor metabolism. In addition, studies have shown that sonic power can also destroy tumor mitochondria, resulting in a decrease in ATP content. MTT assay also showed that BO combined with ultrasound had the best tumor growth inhibition rate (the tumor inhibition rate reached 90%), while BO alone or BP plus US had partial tumor growth inhibition (Figure 3E). We next sought to study the effect of SDT on BO-induced ICD by measuring in vivo CRT expression and HMGB1 release (Figures S8 and S9). CRT expression in US + BO group has a significant difference compared with BO group. In general, BO combined with ultrasound has a good anti-tumor effect in vitro and can inhibit tumor growth and metabolism.

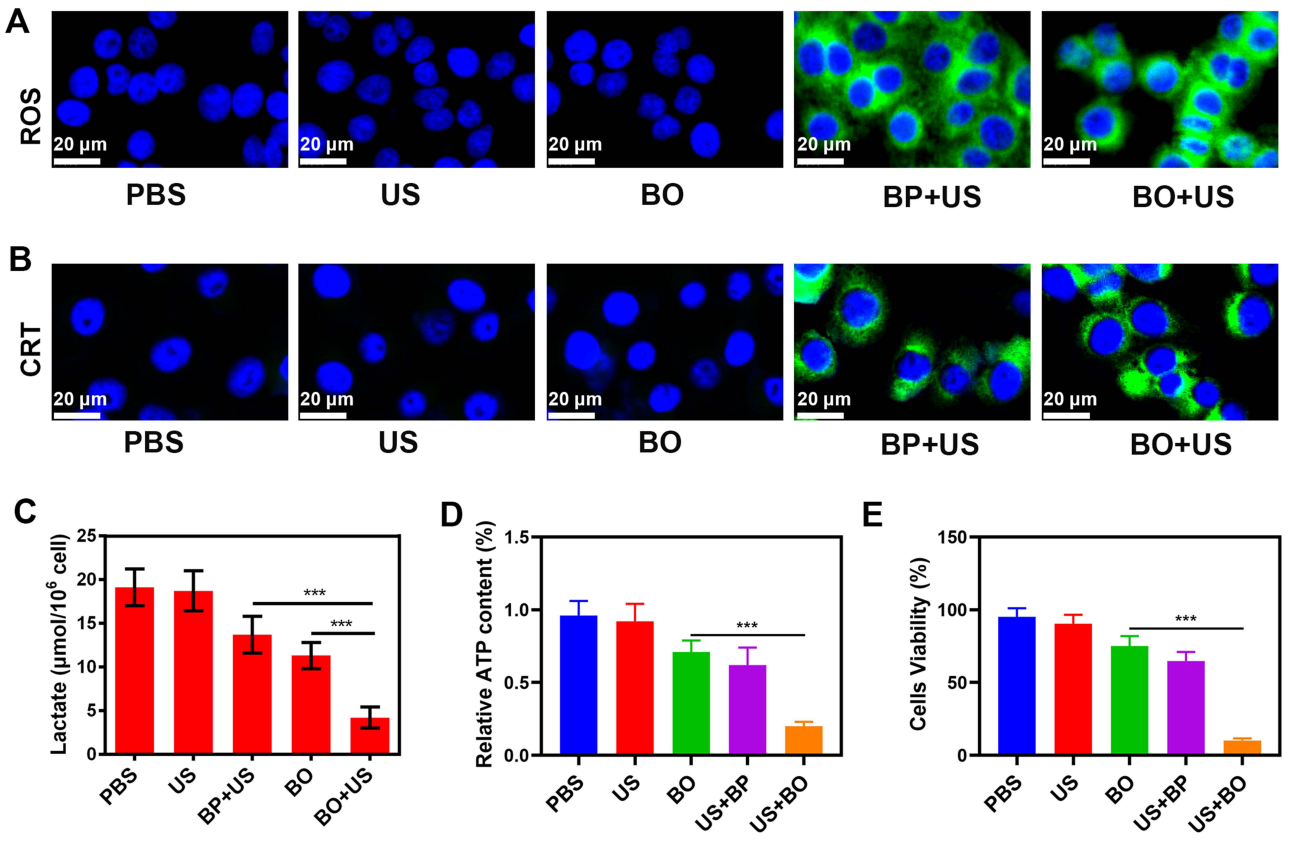

Figure 3 (**A**) Tumor cells DCFH-DA fluorescence images were observed after the indicated treatments. (**B**) Confocal images showing the induction of the ICD marker CRT (stained as green by anti-CRT) on 4T1 cells after different treatments. (**C**) Lactate consumption effect of different formulations in solution. (**D**) ATP inhibition ability of different formulations. (**E**) In vitro cytotoxicity of different formulations against 4T1 cells. ***P < 0.005; Student's *t*-test.

In vivo Intensification of Vascular Damage Effects of BO System

Given that flow cytometry analysis of the frequency of CRT^+ tumor cells in vitro showed profound ICD upon BO treatment when combined with appropriate SDT. We further explore in vivo intensification of vascular damage effects. Immunofluorescence micrographs in Figure 4A clearly demonstrated that US + BP treatment would cause high expression of CD31 (a typical vascular marker), the expression of CD31 in US + BO was obviously down-regulated with a significant difference compared to only BO treated group. Furthermore, the formation of hypoxia in the tumor microenvironment is related to many factors, one of which is blood vessels, which carry an amount of hemoglobin. Also, a large number of blood vessels will also be beneficial to tumor metastasis and recurrence. As shown in Figure 4B, intratumoral hypoxia area was reduced in the combination treatment of BO, the increased PIMO fluorescence in US + BO group could be attributed to the complex function of O_2 consumption by SDT and broken of blood vessels. The corresponding quantitative analysis (Figure 4C and D) in Figure 4A and B also confirmed the consistent conclusion. Next, lactic acid consumption effect of the BO nanosystem was evaluated at in vivo animal model (Figure 4E). After 12 h treatment of BO, the lactate content (mg/g tumor) declined from about 35.4 (mg/g tumor) to 22.5 (mg/g tumor), while synergistic BO with appropriate intensity of US exert a more potent inhibition to lactic acid content in tumor site, only after 3 h of processing, lactate content dropped rapidly from about 35.8 (mg/g tumor) to 10.4 (mg/g tumor), and it dropped to less than 9.0 after combined treatment of 12 h. As SDT disrupts angiogenesis, and 3PO inhibits the biochemical process of glycolysis, which makes it difficult for tumor cells to absorb glucose and convert it into lactic acid. Notably, the in vivo lactate results of BP + US differs from the in vitro experiments, after 3 h of treatment, the lactic acid content in the BP + US group was suppressed (from 35.5 mg/g to 31.5 mg/g), which was attributed to tumor growth suppression conducted by SDT. However, since oxygen was consumed by the sonodynamic therapy, the tumor cells were more inclined to achieve anaerobic respiration, so the lactic acid content around the tumor cells increased sharply to 43.5

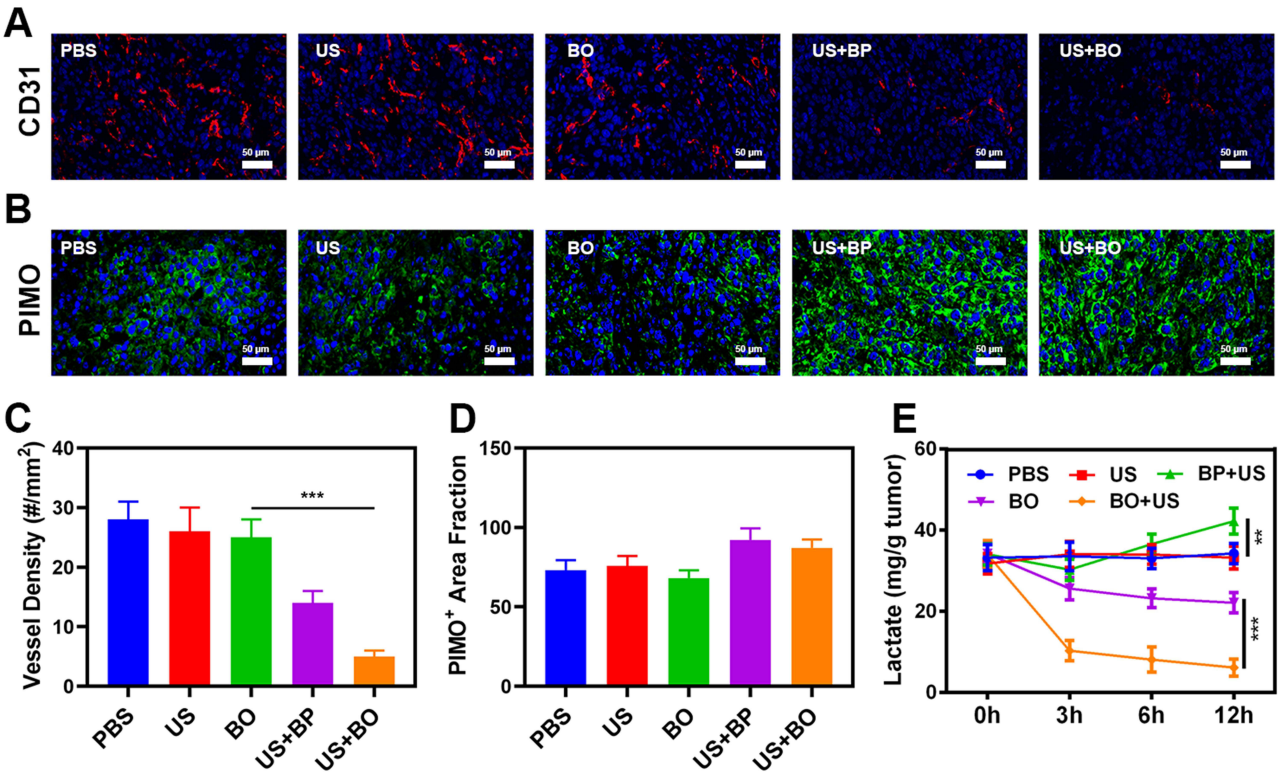

Figure 4 (**A**) CD31 immunofluorescent images following different treatments. (**B**) Representative images of tumor tissue sections stained with anti-PIMO (green) following the indicated treatments. (**C**) Immunohistological quantification of the tumor vessel density, as assessed by the number of vessels normalized to the image area (n = 3). (**D**) Fraction of pimonidazole (PIMO) positive hypoxic area in different groups (n = 3). (**E**) Lactate consumption effect of different in vivo treatments.**P < 0.001, ***P < 0.005; Student's t-test.

(mg/g tumor) after 12 h. However, superfluous lactate would further damage cytotoxic T cells and inhibit the differentiation and maturation of DCs, thus produce restricted immune microenvironment. Hence, our system might improve the tumor immunosuppressive microenvironment and activate systemic tumor immunity.

In vivo Anti-Tumor Study of BO System

We next evaluated BO-mediated SDT efficiency in mice bearing 4T1 tumors. To investigate the abscopal and primary effect of the BO, BALB/c mice were subcutaneous injected with 1×106 4T1 cells into the right flank (primary tumors) and 2×10^5 4T1 cells into the left flank (abscopal tumors), respectively. The mice were grouped and treated when the primary tumor volume reached 200 mm^3. Tumor bearing mice were divided randomly into 5 groups (each group included 5 mice): (1) PBS; (2) US; (3) BO; (4) BP + US (5) BO + US. The equivalent 3PO dose was 3.4 mg/kg in group 3, 4 and 5. After 12 h of intravenous injection, US irradiation (power density = 0.75 W cm^{-2}, transducer frequency = 1 MHz, 30% duty cycle, 10 min) was carried out. The treatment was conducted every 4 days for 13 days, treatment schedule was shown in Figure 5A. During the 2 weeks treatment, the primary and abscopal tumor volumes of only US or BO treated group rose rapidly, as shown in Figure 5B and C. the group of US combined with BP exhibited a minor inhibitory effect to primary, as US could induce ROS generation from BP sonosensitizers and cause a moderate damage to primary tumors. However, a weak immune system leaves the growth curve of abscopal tumor hardly changed at all. Notably, Because BO combined with ultrasound treatment inhibited the production of lactic acid and changed the low-activity immune environment, dendritic cells in lymph nodes were activated, which could efficiently absorb, process and present antigens and attract to tumor tissue to activate initial T cells. As this combination therapy further cuts off the source of ATP, thus achieving potent starvation therapy and immunotherapy. After the mice were finally sacrificed, the mass of primary and distal tumors in BO + US group was only 0.1 g and 0.36 g (Figure 5D and E), respectively, which was consistent with the curve of tumor volume (Figure S19). We took tumor tissue sections for various staining. Ki-67 staining (Figure S10) also confirmed that there was almost no proliferation of primary tumor cells, and TUNEL and H&E staining (Figures S11 and S12) confirmed that there was a large amount of cell necrosis in the BO + US treatment

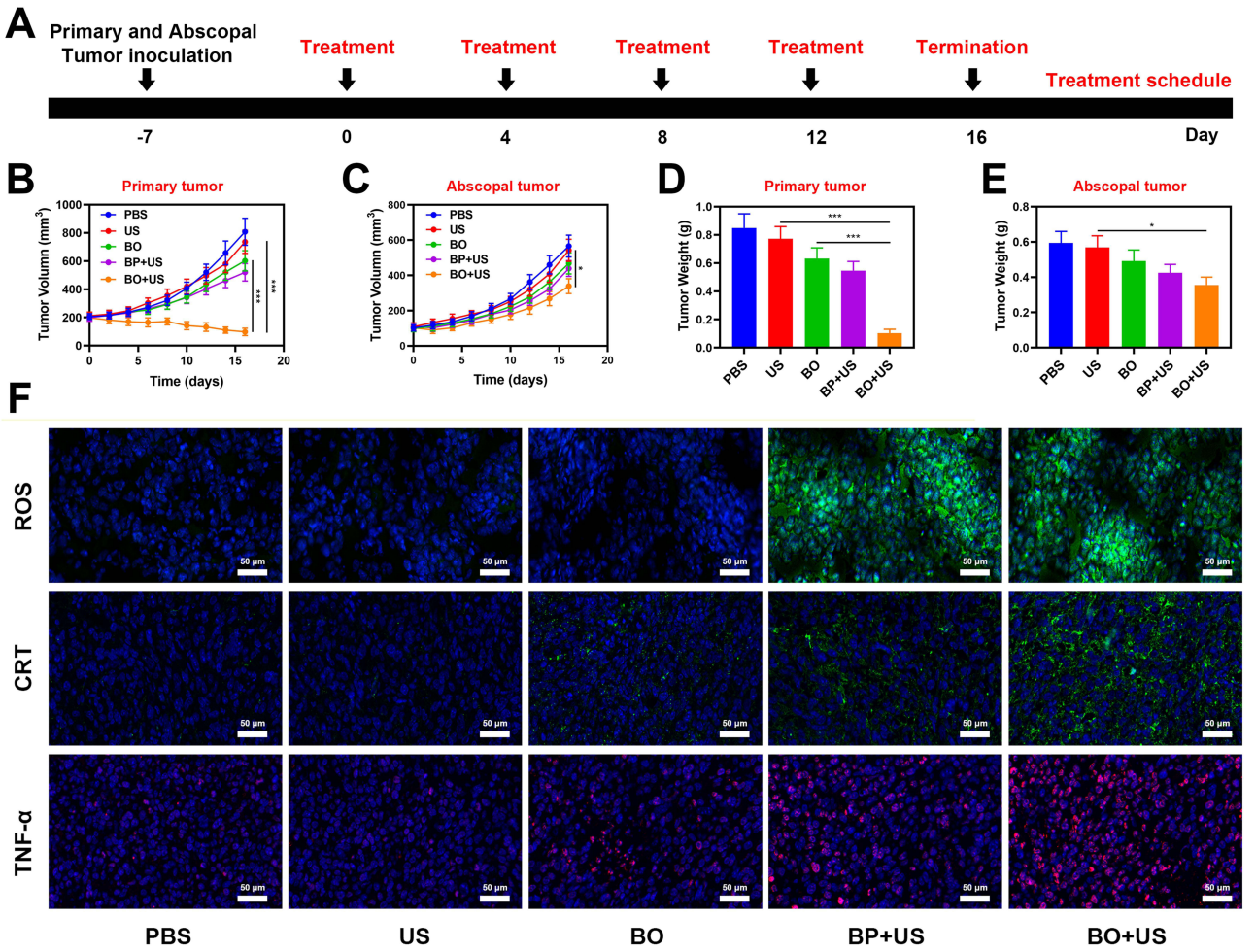

Figure 5 (**A**) Treatment schedule for US and BO combination therapy. (**B**) Changes in primary tumor volume over time in response to the indicated treatments. (**C**) Changes in abscopal tumor volume over time in response to the indicated treatments. (**D**) Average primary tumor weight values following the indicated treatments. (**E**) Average abscopal tumor weight values following the indicated treatments. (**F**) CLSM examination of CRT exposure, TNF-α stained tumor sections and ROS generation from the indicated treatment groups. *P < 0.05, ***P < 0.005; Student's t-test.

group. The production of ROS in the primary tumors of the treated mice was detected using DCF fluorescent probe, indicating that the tumor staining was significantly enhanced in the mice treated with the combination therapy about BO + US. Thus, enhancing free radical generation and improving SDT activity resulted in stronger efficacy to these animals as ROS can induce oxidative stress to promote apoptosis and necrosis, thereby accelerating the death of tumor cells. The body weight of the mice during the treatment period was almost normal in all groups, indicating the biosafety of our treatment approach (Figure S13). CRT exposure and TNF-α stained tumor sections from the indicated treatment groups also verified BO-mediated SDT and starvation therapy (Figure 5F). In the process of maturation, DCs migrate from peripheral tissues that contact antigen to secondary lymphatic organs, contact with T cells and stimulate immune response. DC, as the most functional APC found so far, can induce the formation of specific cytotoxic T lymphocyte (CTL).[47] The maturation of a large number of DCs also indirectly increases the $CD8^+$ content, the immunofluorescence showing CD4+ and CD8+ T cells increased in BO+US group (Figures S17). The activation of a large number of T cells means the activation of the systemic immune system, and the T cells are constantly free and search for foreign invaders to kill, which also leads to inhibition of abscopal tumor in BO synergistic with US group. The secretion of IL-12p70, tumor necrosis factor-α (TNF-α) and interferon-γ (IFN-γ) appeared to be much higher at BO+US group than other group, favoring for triggering the antitumor immunity (Figures S14–S16). As known, DCs plays a key role in T cells mediated anti-tumor responses, the mature rate of DC was 38.4% ± 3.2% in BO + US group by flow cytometry analysis, as shown in Figure S18. The distribution and metabolism of the drug (BO) in the body was shown in Figures S20. What is more, Immune activation did not cause any loss to systems, as shown in Figures S21–S24, after the

treatment of mice vital organs (heart, liver, spleen, lungs and kidney) without any inflammation and damage in the body, blood biochemistry analysis also indicates the normal liver-kidney index. As many nanomaterials possess great therapeutic efficacy, they are also associated with systemic toxicity, which limits their future clinical applications.[48–50] The in vivo results demonstrate that our novel combined treatment not only achieve a good biological safety therapy but reduce the tumor lactic acid content, cutting off the nutrition supply with profound immunotherapy.

Conclusions

In conclusion, we have designed a glycolysis inhibitor (3PO) loaded and PEG modified black phosphorus nanosheets (BO) for potent starvation therapy and efficient immune activation. Under ultrasound irradiation, the BO can produce ROS to destroy tumors and tumor blood vessels and lead to further hypoxia and nutrients block. Then, the released 3PO inhibits tumor glycolysis and prevents the hypoxia-induced glycolysis and lactate accumulation. Both SDT and 3PO can cut off the source of lactic acid, as well as achieve antitumor starvation therapy through the blockade of the adenosine triphosphate (ATP) supply. In addition, the combination of lactate depletion and SDT further facilitates dendritic cells (DC) maturation, promotes antigen presentation by DCs, and eventually propagates the antitumor immunity and inhibition of abscopal tumor growth. This is the first time that combines SDT with inhibition of glycolysis, achieving admirable tumor treatment and decreasing adverse events caused by SDT process. Our system provides a new idea for the future design of anti-tumor nanomedicines. In the future, BO system will definitely be combined with immune antibodies, such as PD-1 and CD47 antibodies, to achieve better immunotherapeutic effect, and we will pay attention to its effect on tumor recurrence.

Data Sharing Statement

Other experimental details can be found in the supporting information section.

Acknowledgments

This work was supported by the Guangxi Natural Science Foundation under Grant No.2023GXNSFBA026137, the Haiyan Foundation of Harbin Medical University Cancer Hospital (Grant Number: JJQN2022-01), the China Postdoctoral Science Foundation (2022M710853 to Y. Pan) and Beijing Cancer Prevention & Treatment Society (IZXUEYANZI2022-1004).

Disclosure

The authors declare no competing financial interest.

References

1. Zhu D, Lyu M, Huang Q, et al. Stellate plasmonic exosomes for penetrative targeting tumor NIR-II thermo-radiotherapy. *ACS Appl Mater Interfaces*. 2020;12(33):36928–36937. doi:10.1021/acsami.0c09969
2. Zhu D, Liu Z, Li Y, Huang Q, Xia L, Li K. Delivery of manganese carbonyl to the tumor microenvironment using tumor-derived exosomes for cancer gas therapy and low dose radiotherapy. *Biomaterials*. 2021;274:120894. doi:10.1016/j.biomaterials.2021.120894
3. Mao Y, Zou C, Jiang Y, Fu D. Erythrocyte-derived drug delivery systems in cancer therapy. *Chin Chem Lett*. 2021;32(3):990–998. doi:10.1016/j.cclet.2020.08.048
4. Duo Y, Zhu D, Sun X, et al. Patient-derived microvesicles/AIE luminogen hybrid system for personalized sonodynamic cancer therapy in patient-derived xenograft models. *Biomaterials*. 2021;272:120755. doi:10.1016/j.biomaterials.2021.120755
5. Jiang F, Yang C, Ding B, et al. Tumor microenvironment-responsive MnSiO3-Pt@BSA-Ce6 nanoplatform for synergistic catalysis-enhanced sonodynamic and chemodynamic cancer therapy. *Chin Chem Lett*. 2022;33:2959–2964. doi:10.1016/j.cclet.2021.12.096
6. Wang X, Zhong X, Bai L, et al. Ultrafine titanium monoxide (TiO1+x) nanorods for enhanced sonodynamic therapy. *J Am Chem Soc*. 2020;142(14):6527–6537. doi:10.1021/jacs.9b10228
7. Xiao Z, Chen Q, Yang Y, et al. State of the art advancements in sonodynamic therapy (SDT): metal-Organic frameworks for SDT. *J Chem Eng*. 2022;449:137889. doi:10.1016/j.cej.2022.137889
8. Wang X, Zhong X, Cheng L. Titanium-based nanomaterials for cancer theranostics. *Coord Chem Rev*. 2021;430:213662. doi:10.1016/j.ccr.2020.213662
9. Zhu J, Ouyang A, Shen Z, et al. Sonodynamic cancer therapy by novel iridium-gold nanoassemblies. *Chin Chem Lett*. 2021;2012:1.
10. Qian X, Zheng Y, Chen Y. Micro/Nanoparticle-Augmented Sonodynamic Therapy (SDT): breaking the depth shallow of photoactivation. *Adv Mater*. 2016;28(37):8097–8129. doi:10.1002/adma.201602012

11. Zhang T, Zhang J, Wang FB, et al. Mitochondria-targeting phototheranostics by aggregation-Induced NIR-II emission luminogens: modulating intramolecular motion by electron acceptor engineering for multi-modal synergistic therapy. *Adv Funct Mater*. 2022;32:2110526. doi:10.1002/adfm.202110526
12. Zhu D, Zheng Z, Luo G, et al. Single injection and multiple treatments: an injectable nanozyme hydrogel as AIEgen reservoir and release controller for efficient tumor therapy. *Nano Today*. 2021;37:101091. doi:10.1016/j.nantod.2021.101091
13. Son S, Kim JH, Wang X, et al. Multifunctional sonosensitizers in sonodynamic cancer therapy. *Chem Soc Rev*. 2020;49:3244–3261. doi:10.1039/C9CS00648F
14. Huang C, Ding S, Jiang W, Wang F-B. Glutathione-depleting nanoplatelets for enhanced sonodynamic cancer therapy. *Nanoscale*. 2021;13(8):4512–4518. doi:10.1039/D0NR08440A
15. Sun Y, Wang H, Wang P, et al. Tumor targeting DVDMS-nanoliposomes for an enhanced sonodynamic therapy of gliomas. *Biomater Sci*. 2019;7(3):985–994. doi:10.1039/C8BM01187G
16. Liu Q, Shi L, Liao Y, et al. Ultrathin-FeOOH-Coated MnO 2 sonosensitizers with boosted reactive oxygen species yield and remodeled tumor microenvironment for efficient cancer therapy. *Adv Sci*. 2022;9:e2200005. doi:10.1002/advs.202200005
17. Liang S, Deng X, Chang Y, et al. Intelligent Hollow Pt-CuS janus architecture for synergistic catalysis-enhanced sonodynamic and photothermal cancer therapy. *Nano Lett*. 2019;19(6):4134–4145. doi:10.1021/acs.nanolett.9b01595
18. Wang X, Wang Q, Yue H, et al. Liquid exfoliation of TiN nanodots as novel sonosensitizers for photothermal-enhanced sonodynamic therapy against cancer. *Nano Today*. 2021;39:101170. doi:10.1016/j.nantod.2021.101170
19. Gao F, Tang Y, Liu WL, et al. Intra/Extracellular lactic acid exhaustion for synergistic metabolic therapy and immunotherapy of tumors. *Adv Mater*. 2019;31:e1904639. doi:10.1002/adma.201904639
20. Suveera D, Rajesh Kumar D, Paolo Ettore P, Pierre S. Multiple biological activities of lactic acid in cancer: influences on tumor growth, angiogenesis and metastasis. *Curr Pharm Des*. 2012;18(10):1319–1330. doi:10.2174/138161212799504902
21. Chen Z-X, Liu M-D, Zhang M-K, et al. Interfering with lactate-fueled respiration for enhanced photodynamic tumor therapy by a porphyrinic MOF nanoplatform. *Adv Funct Mater*. 2018;28(36):1803498. doi:10.1002/adfm.201803498
22. Altman BJ, Stine ZE, Dang CV. From Krebs to clinic: glutamine metabolism to cancer therapy. *Nat Rev Cancer*. 2016;16(10):619–634.
23. Wang X, Zhao Y, Shi L, et al. Tumor-targeted disruption of lactate transport with reactivity-reversible nanocatalysts to amplify oxidative damage. *Small*. 2021;17:2100130. doi:10.1002/smll.202100130
24. Li SY, Cheng H, Xie BR, et al. Cancer cell membrane camouflaged cascade bioreactor for cancer targeted starvation and photodynamic therapy. *ACS nano*. 2017;11(7):7006–7018. doi:10.1021/acsnano.7b02533
25. Shen L, Zhou T, Fan Y, et al. Recent progress in tumor photodynamic immunotherapy. *Chin Chem Lett*. 2020;31(7):1709–1716. doi:10.1016/j.cclet.2020.02.007
26. Yu X, Ma H, Xu G, Liu Z. Radiotherapy assisted with biomaterials to trigger antitumor immunity. *Chin Chem Lett*. 2022;33:4169–4174. doi:10.1016/j.cclet.2022.02.049
27. Jiang N, Zhou Z, Xiong W, et al. Tumor microenvironment triggered local oxygen generation and photosensitizer release from manganese dioxide mineralized albumin-ICG nanocomplex to amplify photodynamic immunotherapy efficacy. *Chin Chem Lett*. 2021;32(12):3948–3953. doi:10.1016/j.cclet.2021.06.053
28. Yang Y, Zhao T, Chen Q, et al. Nanomedicine strategies for heating "Cold" Ovarian Cancer (OC): next evolution in immunotherapy of OC. *Adv Sci*. 2022;9(28):e2202797. doi:10.1002/advs.202202797
29. Yang Y, Huang J, Liu M, et al. Emerging sonodynamic therapy-based nanomedicines for cancer immunotherapy. *Adv Sci*. 2023;10(2):e2204365. doi:10.1002/advs.202204365
30. Colegio OR, Chu N-Q, Szabo AL, et al. Functional polarization of tumour-associated macrophages by tumour-derived lactic acid. *Nature*. 2014;513(7519):559–563. doi:10.1038/nature13490
31. Zhu D, Chen H, Huang C, et al. H_2O_2 Self-producing single-atom nanozyme hydrogels as light-controlled oxidative stress amplifier for enhanced synergistic therapy by transforming "cold" tumors. *Adv Funct Mater*. 2022;32(16):2110268. doi:10.1002/adfm.202110268
32. Zhu Y, Wang Z, Zhao R, et al. Pt Decorated Ti(3)C(2)T(x) MXene with NIR-II light amplified nanozyme catalytic activity for efficient phototheranostics. *ACS nano*. 2022;16(2):3105–3118. doi:10.1021/acsnano.1c10732
33. Zhao T, Wu W, Sui L, et al. Reactive oxygen species-based nanomaterials for the treatment of myocardial ischemia reperfusion injuries. *Bioact Mater*. 2022;7:47–72. doi:10.1016/j.bioactmat.2021.06.006
34. Chen L, Huang Q, Zhao T, et al. Nanotherapies for sepsis by regulating inflammatory signals and reactive oxygen and nitrogen species: new insight for treating COVID-19. *Redox Biol*. 2021;45:102046. doi:10.1016/j.redox.2021.102046
35. Zhu Y, Zhao T, Liu M, et al. Rheumatoid arthritis microenvironment insights into treatment effect of nanomaterials. *Nano Today*. 2022;42:101358.
36. Huang J, He B, Zhang Z, et al. Aggregation-induced emission luminogens married to 2D black phosphorus nanosheets for highly efficient multimodal theranostics. *Adv Mater*. 2020;32:2003382. doi:10.1002/adma.202003382
37. Liu J, Liu T, Du P, Zhang L, Lei J. Metal-Organic Framework (MOF) hybrid as a tandem catalyst for enhanced therapy against hypoxic tumor cells. *Angew Chem*. 2019;58(23):7808–7812. doi:10.1002/anie.201903475
38. Guo T, Wu Y, Lin X, et al. Black phosphorus quantum dots with renal clearance property for efficient photodynamic therapy. *Small*. 2018;14(4):1702815. doi:10.1002/smll.201702815
39. Cheng L, Qiu S, Wang J, et al. A multifunctional nanocomposite based on Pt-modified black phosphorus nanosheets loading with l-arginine for synergistic gas-sonodynamic cancer therapy. *Colloids Surf a Physicochem Eng Asp*. 2022;638:128284. doi:10.1016/j.colsurfa.2022.128284
40. Li Z, Zhang T, Fan F, et al. Piezoelectric materials as sonodynamic sensitizers to safely ablate tumors: a case study using black phosphorus. *J Phys Chem Lett*. 2020;11(4):1228–1238. doi:10.1021/acs.jpclett.9b03769
41. Chen B-Q, Kankala RK, Zhang Y, et al. Gambogic acid augments black phosphorus quantum dots (BPQDs)-based synergistic chemo-photothermal therapy through downregulating heat shock protein expression. *J Chem Eng*. 2020;390:124312. doi:10.1016/j.cej.2020.124312
42. Chan L, Gao P, Zhou W, et al. Sequentially triggered delivery system of black phosphorus quantum dots with surface charge-switching ability for precise tumor radiosensitization. *ACS nano*. 2018;12:12401–12415. doi:10.1021/acsnano.8b06483
43. Ou W, Byeon JH, Soe ZC, et al. Tailored Black phosphorus for erythrocyte membrane nanocloaking with interleukin-1alpha siRNA and paclitaxel for targeted, durable, and mild combination cancer therapy. *Theranostics*. 2019;9(23):6780–6796. doi:10.7150/thno.37123

44. Zeng X, Luo M, Liu G, et al. Polydopamine-modified black phosphorous nanocapsule with enhanced stability and photothermal performance for tumor multimodal treatments. *Adv Sci*. 2018;5(10):1800510. doi:10.1002/advs.201800510
45. Yuan M, Liang S, Zhou Y, et al. A robust oxygen-carrying hemoglobin-based natural sonosensitizer for sonodynamic cancer therapy. *Nano Lett*. 2021;21:6042–6050. doi:10.1021/acs.nanolett.1c01220
46. Sun S, Xu Y, Fu P, et al. Ultrasound-targeted photodynamic and gene dual therapy for effectively inhibiting triple negative breast cancer by cationic porphyrin lipid microbubbles loaded with HIF1alpha-siRNA. *Nanoscale*. 2018;10(42):19945–19956. doi:10.1039/C8NR03074J
47. Zhou F, Feng B, Yu H, et al. Tumor microenvironment-activatable prodrug vesicles for nanoenabled cancer chemoimmunotherapy combining immunogenic cell death induction and CD47 blockade. *Adv Mater*. 2019;31:e1805888. doi:10.1002/adma.201805888
48. Zhu D, Zhang T, Li Y, et al. Tumor-derived exosomes co-delivering aggregation-induced emission luminogens and proton pump inhibitors for tumor glutamine starvation therapy and enhanced type-I photodynamic therapy. *Biomaterials*. 2022;283:121462. doi:10.1016/j.biomaterials.2022.121462
49. Zhu D, Zhang J, Luo G, Duo Y, Tang BZ. Bright bacterium for hypoxia-tolerant photodynamic therapy against orthotopic colon tumors by an interventional method. *Adv Sci*. 2021;8(15):2004769. doi:10.1002/advs.202004769
50. Zhu D, Duo Y, Meng S, et al. Tumor-exocytosed exosome/aggregation-induced emission luminogen hybrid nanovesicles facilitate efficient tumor penetration and photodynamic therapy. *Angew Chem*. 2020;59:2–10.